SANDIA REPORT

SAND87—0959 • UC—705
Unlimited Release
Printed May 1990

The Prediction of Loads on Penetrators Into Rock Via the Spherical Cavity Expansion Approximation

Donald B. Longcope, Jr.

Prepared by
Sandia National Laboratories
Albuquerque, New Mexico 87185 and Livermore, California 94550
for the United States Department of Energy
under Contract DE-AC04-76DP00789

When printing a copy of any digitized SAND Report, you are required to update the markings to current standards.

SF2900Q(8-81)

Issued by Sandia National Laboratories, operated for the United States Department of Energy by Sandia Corporation.

NOTICE: This report was prepared as an account of work sponsored by an agency of the United States Government. Neither the United States Government nor any agency thereof, nor any of their employees, nor any of their contractors, subcontractors, or their employees, makes any warranty, express or implied, or assumes any legal liability or responsibility for the accuracy, completeness, or usefulness of any information, apparatus, product, or process disclosed, or represents that its use would not infringe privately owned rights. Reference herein to any specific commercial product, process, or service by trade name, trademark, manufacturer, or otherwise, does not necessarily constitute or imply its endorsement, recommendation, or favoring by the United States Government, any agency thereof or any of their contractors or subcontractors. The views and opinions expressed herein do not necessarily state or reflect those of the United States Government, any agency thereof or any of their contractors.

Printed in the United States of America. This report has been reproduced directly from the best available copy.

Available to DOE and DOE contractors from
Office of Scientific and Technical Information
PO Box 62
Oak Ridge, TN 37831

Prices available from (615) 576-8401, FTS 626-8401

Available to the public from
National Technical Information Service
US Department of Commerce
5285 Port Royal Rd
Springfield, VA 22161

NTIS price codes
Printed copy: A03
Microfiche copy: A01

SAND87-0959
Unlimited Release
May 1990

Distribution
Category UC-705

THE PREDICTION OF LOADS ON PENETRATORS INTO ROCK VIA THE SPHERICAL CAVITY EXPANSION APPROXIMATION

Donald B. Longcope, Jr.
Applied Mechanics Division IV
Sandia National Laboratories
Albuquerque, New Mexico 87185

ABSTRACT

A spherical cavity expansion (SCE) model for axial loads on penetrators into rock has been developed and used in the GNOME penetrator code to calculate a recent full-scale strategic earth penetrator test (SEPW) into sidewinder tuff. The 2-D target motion is approximated by the 1-D motion produced by an expanding spherical cavity which allows rapid calculations over a complete penetrator trajectory. The target response includes a region of tensile fracturing which has not been modeled in production continuum dynamics code calculations. One reason for the development of this model is the current interest in blunter nosed penetrators than those previously analyzed with cylindrical cavity expansion (CCE) load models.

ACKNOWLEDGMENTS

The author thanks Bob Kipp, Division 1522, for implementing a portion of the SCE load subroutine into GNOME and Mike Forrestal, Division 9123, for helpful suggestions and for pointing out limitations of the quasistatic solutions.

CONTENTS

Introduction 7

SCE Kinematics and Penetrator Nose Geometry 8

Material Model and Response Regions 9

Comparison of SCE and CCE Stresses on the SEPW 10

Comparison of SCE Theory with the SEPW-DG4 Test 11

References 13

Appendix - Solution of Spherical Expansion Problems 21

Governing Equations 21

Quasistatic Response 22

Dynamic Elastic-Plastic Response 24

Dynamic Elastic-Cracked-Plastic Response 27

Use of the SCE Model as a Load Subroutine 29

FIGURES

1. Spherical Cavity Expansion and Penetrator Nose Geometry 14

2. Pressure - Volume Strain Data for Sidewinder Tuff and the Linear Hydrostat 15

3. Triaxial Strength Data for Sidewinder Tuff and the Mohr-Coulomb Failure Criterion 16

4. Spherical Cavity Expansion Response Regions 17

5. Comparison of SCE and CCE Load Models for a Cone with $\ell/d = 1$ into Sidewinder Tuff 18

6. Geometry of Full-Scale SEPW Used in SEPW-D64 Test 19

7. SCE and CCE Calculated and Measured Axial Deceleration for the SEPW-D64 Test 20

INTRODUCTION

A spherical cavity expansion (SCE) model for loads on penetrators into rock and other geologic media has been developed and implemented into the GNOME penetrator code, Reference [1]. The spherical and cylindrical cavity expansion (CCE) load models use results from 1-D wave propagation problems which approximate the 2-D or 3-D target motion. These load models have been used in GNOME to rapidly calculate complete penetration trajectories, and are well-suited to investigate the effects of target property uncertainties and penetrator design changes. The SCE load model was developed because of current interest in the Strategic Earth Penetrator Weapon (SEPW) which has a 3.0 CRH (caliber radius head) ogival nose. This nose is considerably blunter than those of other recent Sandia penetrators, such as the Pershing-II which had a 6.0 CRH nose. The SCE model may be better-suited for the SEPW than existing CCE models, References [2,3], because the SCE kinematics represents both vertical and radial target motion whereas the CCE model allows only radial motion and breaks down in the limit of a very blunt nose.

Some related previous work includes Reference [2] which numerically solved 1-D, nonlinear, dynamic cylindrical cavity expansion problems. References [3,4] developed CCE and SCE results using approximate solution techniques. Reference [5] developed the first SCE load model used in GNOME which approximated the target response as rigid-plastic. Reference [6] used the continuum dynamics code PRONTO to calculate penetration events with a 2-D, elastic-plastic target response model.

The present work follows the solution technique of Reference [2]. It represents the target with regions of elastic, tensile fractured and Mohr-Coulomb plastic response. Closed-form results for the quasistatic response are developed and used to check the numerical procedure for the dynamic response in the limiting case. A comparison is made between loads calculated with SCE and CCE models which shows significant differences, particularly at low penetrator velocities when tensile cracking is

important. Finally, the SEPW-DG4 test, Reference [7], is calculated with the SCE model in GNOME and found to agree reasonably well with the deceleration-time measurements.

SCE KINEMATICS AND PENETRATOR NOSE GEOMETRY

It is assumed that the projectile impacts a uniform target half-space at normal incidence with velocity V in the vertical, z direction. The target response is axisymmetric and 2-D. The penetrator nose geometry is axisymmetric, typically either a cone or ogive. The normal stress on the penetrator nose is approximated by the pressure σ required to expand a spherical cavity in an infinite medium, Figure 1. Thus, the 2-D target response is replaced by the 1-D cavity expansion problem. The cavity is assumed to expand from zero initial radius with constant radial velocity, $\dot{a}$, and this requires stress σ on the cavity surface, where σ depends on $\dot{a}$, but not on a. Then the normal stress on the penetrator nose at a particular location, Q in Figure 1, is taken to be σ for a corresponding spherical cavity which is tangent to Q as shown in Figure 1 and is expanding with

$$\dot{a} = V\sin\theta \tag{1}$$

where $V\sin\theta$ is the component of penetrator velocity normal to its surface at Q. For a conical nose, the stress is constant over the nose for a given penetrator velocity, while for an ogive nose, the stress is a maximum at the tip and decreases toward the tangent point between the nose and aft-body.

The SCE kinematics represent the target vertical motion as well as its radial motion, whereas CCE allows only radial target motion. Thus the SCE approximation should be better than the CCE for noses which are blunt, while the CCE motion is accurate for slender penetrator noses.

Much of this work is concerned with the solution of the 1-D wave propagation problem for the expanding spherical cavity in an infinite medium represented by appropriate geological material response models.

MATERIAL MODEL AND RESPONSE REGIONS

Material compressibility is modeled by a linear pressure-volume strain relation

$$P = K\eta; \quad P = \frac{1}{3}\left(\sigma_R + 2\sigma_\phi\right); \quad \eta = 1 - \rho_0/\rho \tag{2}$$

where σ_R and $\sigma\phi$ are the radial and tangential components of Cauchy stress, taken positive in compression, in a spherical coordinate system; P is the pressure; K is a constant; η is the volumetric strain; and ρ_0 is the initial density. Figure 2 shows how Equation (2) with K = 91 kbar fits data from Reference [8] for sidewinder tuff, a target of recent SEPW penetrator field tests.

The target shear strength is represented by a pressure-dependent yield or failure condition

$$\sigma_R - \sigma_\phi = \mu P + \tau_0; \quad \tau_0 = (1 - \mu/3)Q \tag{3}$$

where μ and τ_0 are constants and Q is the unconfined compressive strength. Tensile fracture in geologic materials is accounted for by the tensile strength Y and the requirement

$$\sigma_\phi > - Y \tag{4}$$

which insures that the tensile stress not exceed the tensile strength. Equations (3,4) are a Mohr-Coulomb failure criterion with a tensile cutoff. This model with μ = 0.91, Q = 0.50 kbar and Y = 0.033 kbar is compared in Figure 3 with sidewinder tuff data from Reference [8]. The Mohr-Coulomb failure criterion is a generalization of the Tresca yield condition for

metals and is often used as a yield surface to describe the plastic behavior of geologic materials. The Mohr-Coulomb condition depends on the hydrostatic pressure through the parameter μ, but is independent of the plastic deformation. In the solution for a spherical cavity expanding continuously from zero initial radius with constant velocity, it is assumed that once the stress state of a particle reaches the Mohr-Coulomb failure surface, it remains there. This is demonstrated for the case $\mu = 0$ in Reference [9].

At stress states below failure, the response is elastic and is represented by the isotropic Hooke's law with bulk modulus K, the same as in Equation (2) and Poisson's ratio, ν.

For the infinite medium in which a spherical cavity is expanding from zero initial radius with constant radial velocity $\dot{a}$, Figure 1b, this material model generally results in three response regions as indicated in Figure 4. Nearest the cavity is a plastic region in which Equation (3) holds. At larger radii is a region of tensile fracturing in which $\sigma_\phi = 0$ which represents the average effect of radially running tensile fractures, and farthest out is a region of elastic response. The cracked region is significant when both the cavity expansion velocity is low and the material tensile strength is much less than the compressive strength, such as for geologic materials.

COMPARISON OF SCE AND CCE STRESSES ON THE SEPW

Using the SCE solution procedures discussed in the Appendix, the stress σ normal to the surface of a conical nosed penetrator with $\ell/d = 1$ into sidewinder tuff has been calculated as a function of penetrator velocity V, where ℓ is the nose length and d is the aft-body diameter. These results are shown in Figure 5. A cone with $\ell/d = 1$ approximates a 3 CRH ogive, the nose shape of the SEPW. In Figure 5 the penetrator velocity is non-dimensionalized by $c_p = [K/\rho_0]^{1/2}$ which is the elastic-plastic interface speed for 1-D strain elastic-perfectly plastic waves and is of the order of

c_1, the unknown (a priori) speed of the interface bounding the plastic region, Figure 4. The target response is elastic-plastic at the higher penetration speeds and elastic-cracked-plastic at lower speeds.

Figure 5 also shows the stress on the penetrator calculated with the cylindrical cavity expansion (CCE) kinematic approximation and the same target response regions. The CCE solution procedure follows that of Reference [2] with σ_z assumed to be the mean of the other two normal stresses. There are significant differences between the SCE and CCE stresses, particularly at low speeds for which the CCE stress is less than one-half of the SCE stress.

Lastly, Figure 5 shows the SCE and CCE stresses in the quasistatic limit when the response is assumed to be elastic-plastic. A comparison of these values with the other results indicates that the stress is significantly lower when tensile cracking is allowed, particularly for the CCE approximations.

COMPARISON OF SCE THEORY WITH THE SEPW-DG4 TEST

The SCE and CCE based theories are compared with the full scale Davis Gun test of a 3.0 CRH SEPW into sidewinder tuff at the Tonopah Test Range on August 21, 1986, Reference [7].

The penetrator external geometry is a 3.0 CRH ogival nose, a cylindrical aft-body, and a gradual conical flare to the back, as shown in Figure 6. It weighs 906 lbs, which included the weight of an integrated pusher plate. The penetrator was launched with a 0° angle of attack and an 80° impact angle from the horizontal. The measured impact velocity was 1520 ft/sec.

The sidewinder tuff target parameters, Reference [8], used in the theory are ρ_0 = 1.80 gm/cm^3, μ = 0.91, K = 91 kbar, Q = 0.50 kbar, υ = 0.21, and Y = 0.033 kbar.

Figure 7 shows the penetrator axial deceleration history from an on board accelerometer filtered to 2 kHz. The theoretical results are computed with GNOME using the SIG5 (CCE) and SIG6 (SCE) load subroutines with combined elastic-plastic and elastic-cracked-plastic target material response. The theory represents the 3.0 ogival nose, but ignores the gradual aft flare. This is justified by the data which do not indicate a significant increase (or change) in the deceleration on entry of the flare into the target (at about 2.4 msec). Sliding penetrator/target frictional effects are not included in the theory. The peak deceleration is predicted well by either theory; but the later-time deceleration is over predicted by the SCE theory and underpredicted by the CCE theory. Target property uncertainties are sufficient to account for either of the differences between the theories and measurements. The calculated maximum depths are 6.9 ft. and 7.2 ft. for the SCE and CCE theories, respectively; while the measured final depth was 9.6 ft.

REFERENCES

1. Davie, N. T. and Richgels, M. A., "GNOME: An Earth Penetrator Code," SAND82-2358, Sandia National Laboratories, Albuquerque, New Mexico, May 1983.

2. Longcope, D. B. and Forrestal, M. J., "Penetration of Targets Described by a Mohr-Coulomb Failure Criterion with a Tension Cutoff," Journal of Applied Mechanics, Vol. 105, June 1983, pp. 327-333.

3. Forrestal, M. J., "Penetration into Dry Porous Rock," International Journal of Solids and Structures, Vol. 22, No. 12, 1986, pp. 1485-1500.

4. Forrestal, M. J., Okajima, K. and Luk, V. K., "Penetration of 6061-T651 Aluminum Targets with Rigid Long Rods," SAND87-1960J, submitted to Journal of Applied Mechanics, 1987.

5. Priddy, T. G., "Smoothly Waning, Symmetrically Expanding, Cavity Pressure Loads in Earth Materials," SAND82-2054, Sandia National Laboratories, Albuquerque, New Mexico, January 1982.

6. Chen, E. P., "Finite Element Simulation of Penetration into Geological Targets," SAND87-0269, Sandia National Laboratories, Albuquerque, New Mexico, March 1987.

7. Wood, W. R., Report on test SEPW-D64, R804357, Sandia National Laboratories, internal report, Division 5144, September 18, 1986.

8. Sakellarion, Chris, letters on mechanical tests of sidewinder tuff, June 9, 1980, July 22, 1980, and January 8, 1981, Terra Tak, Salt Lake City, Utah.

9. Forrestal, M. J. and Luk, V. K., "Dynamic Spherical Cavity-Expansion in a Compressible Elastic-Plastic Solid," Journal of Applied Mechanics, Vol. 55, pp. 275-279, June 1988.

10. Hill, R., The Mathematical Theory of Plasticity, Oxford University Press, New York, 1983, pp. 97-99.

11. Chadwick, P., "The Quasi-Static Expansion of a Spherical Cavity in Metals and Ideal Soils," Quarterly Journal of Mechanics and Applied Mathematics, Vol. 12, Part 1, 1959, pp. 52-71.

12. Shampine, L. F. and Watts, H. A., "DEPAC - Design of a User Oriented Package of ODE Solvers," SAND79-2374, Sandia National Laboratories, Albuquerque, New Mexico, September 1980.

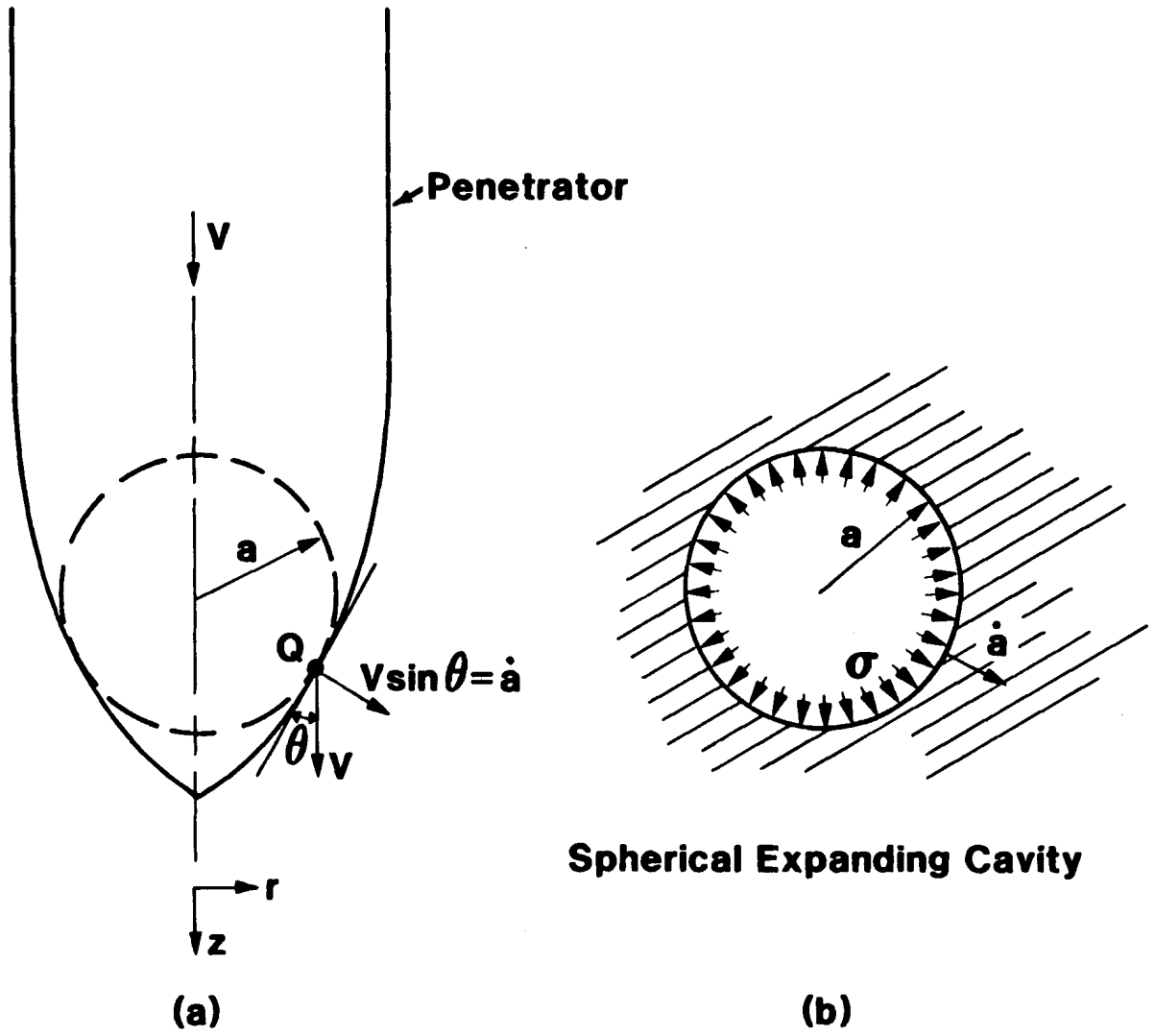

Figure 1. Spherical Cavity Expansion and Penetrator Nose Geometry

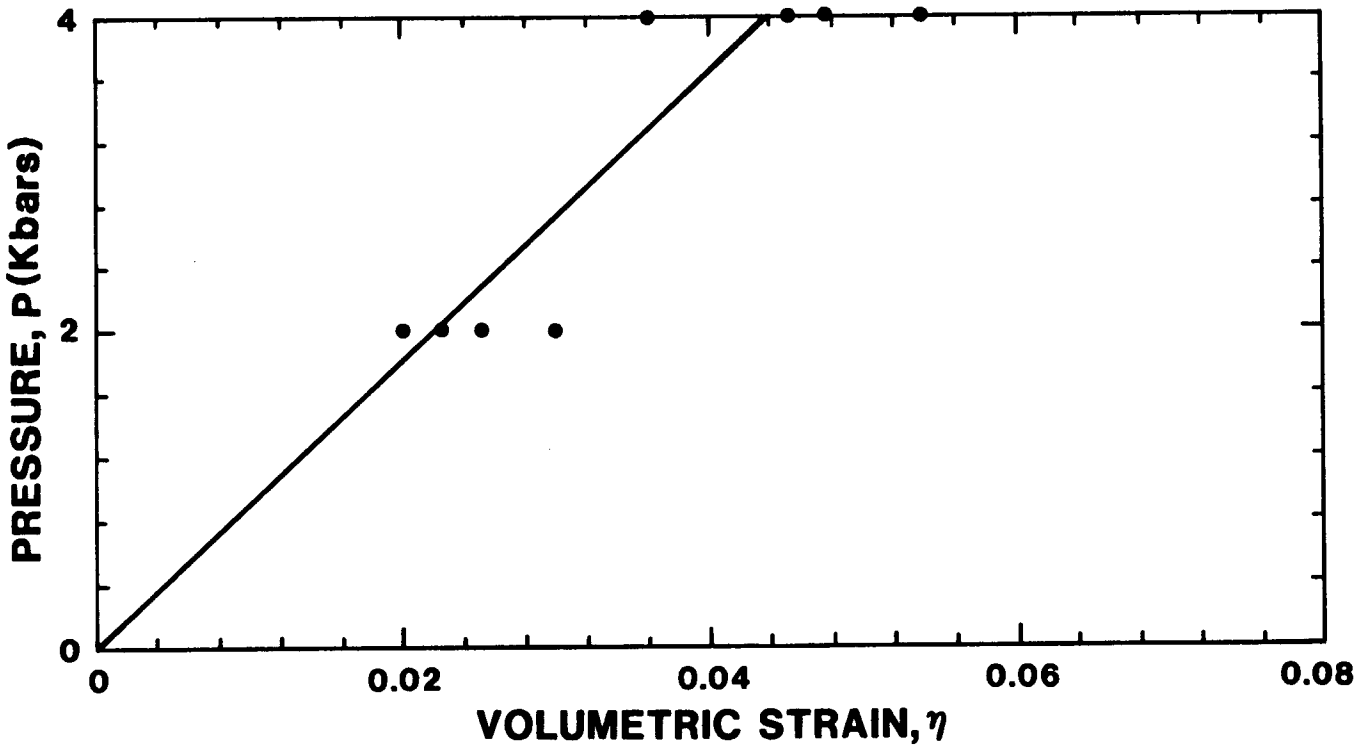

Figure 2. Pressure - Volume Strain Data for Sidewinder Tuff and the Linear Hydrostat

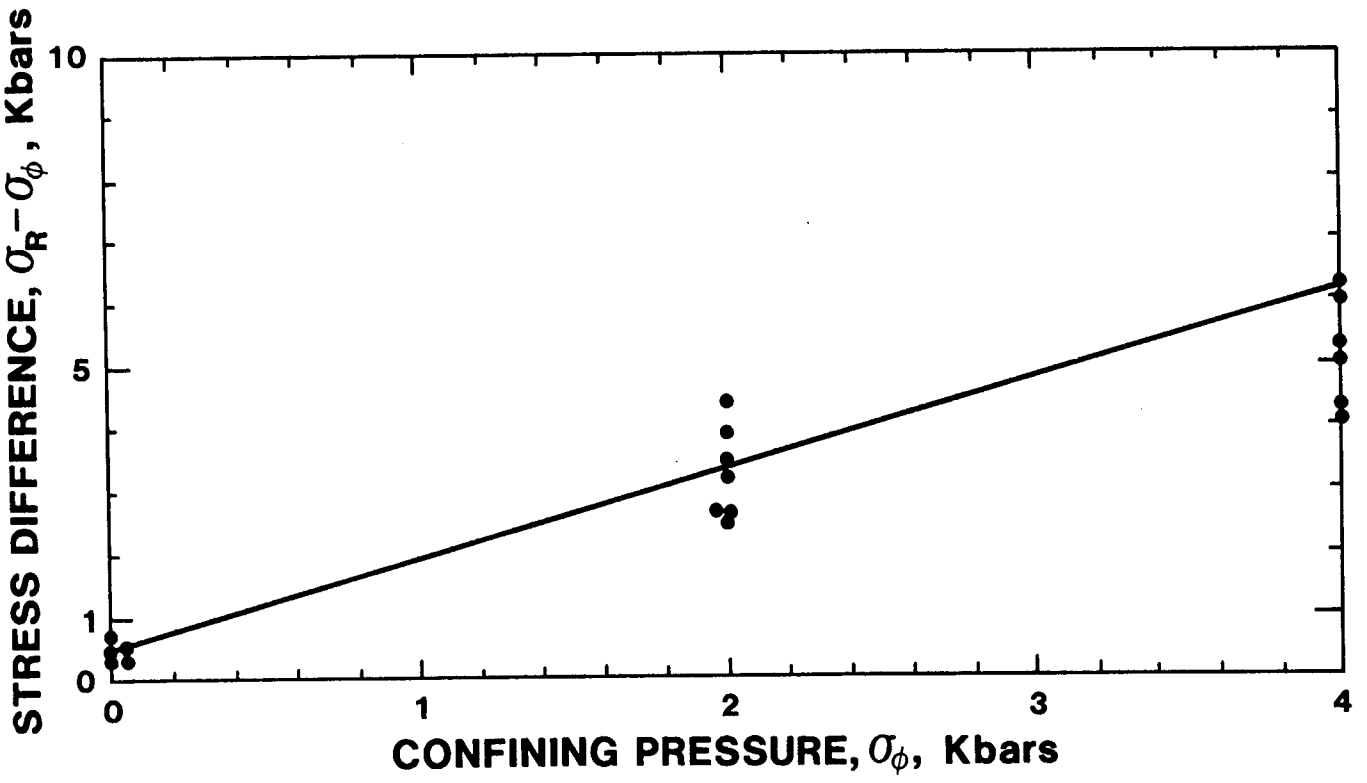

Figure 3. Triaxial Strength Data for Sidewinder Tuff and the Mohr-Coulomb Failure Criterion

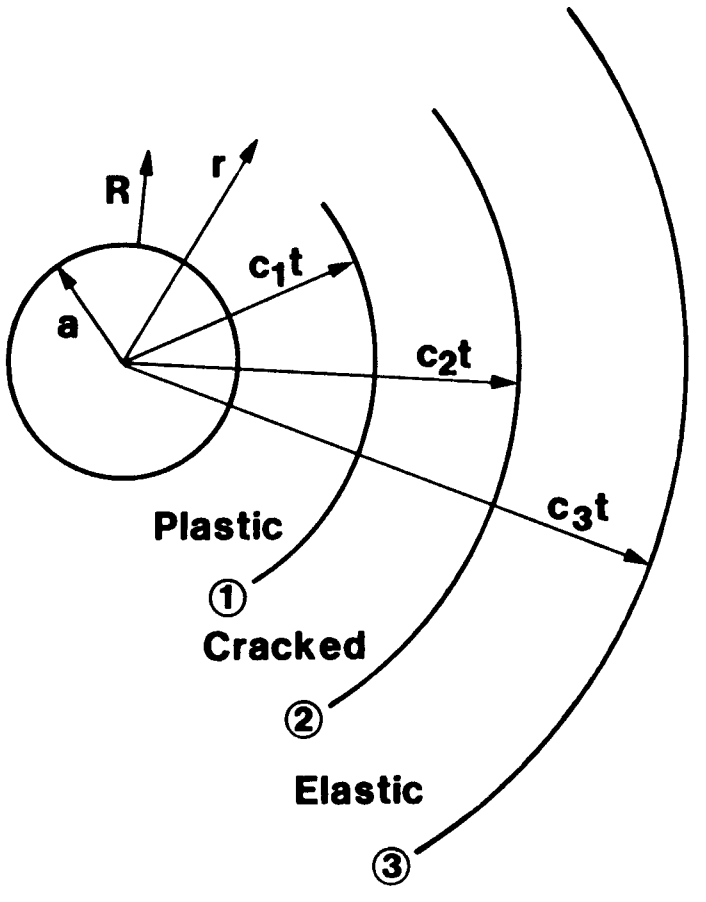

Figure 4. Spherical Cavity Expansion Response Regions

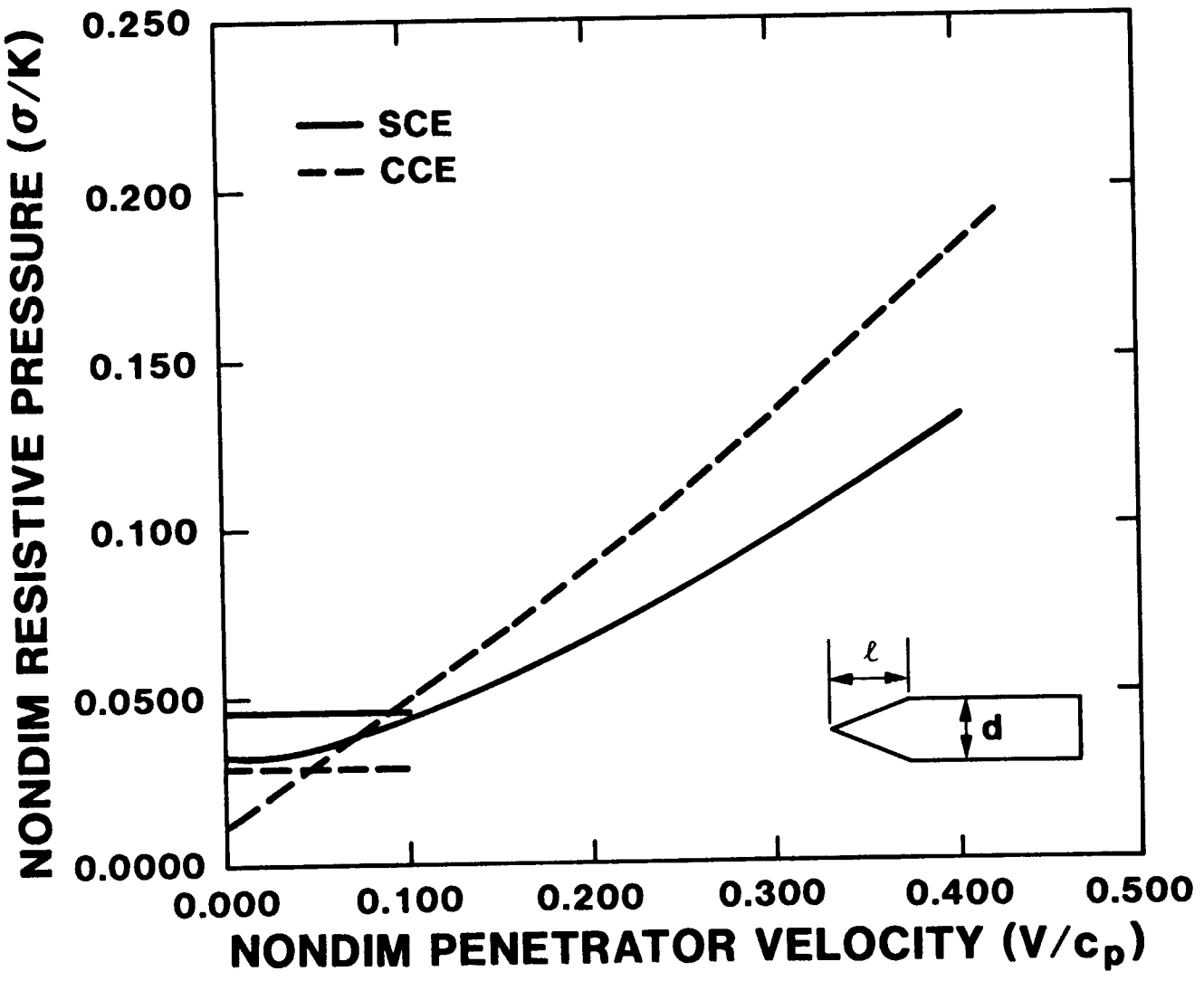

Figure 5. Comparison of SCE and CCE Load Models for a Cone with $\ell/d = 1$ into Sidewinder Tuff

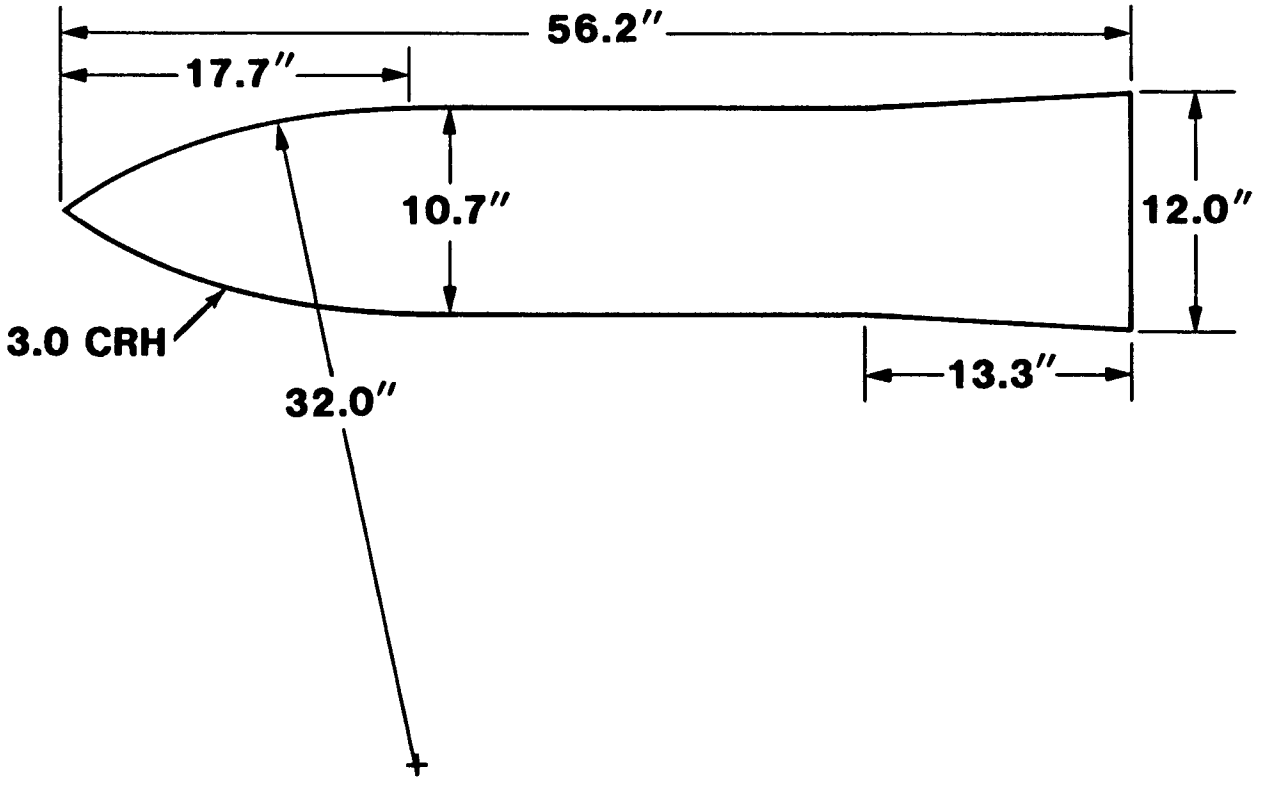

Figure 6. Geometry of Full-Scale SEPW Used in SEPW-DG4 Test

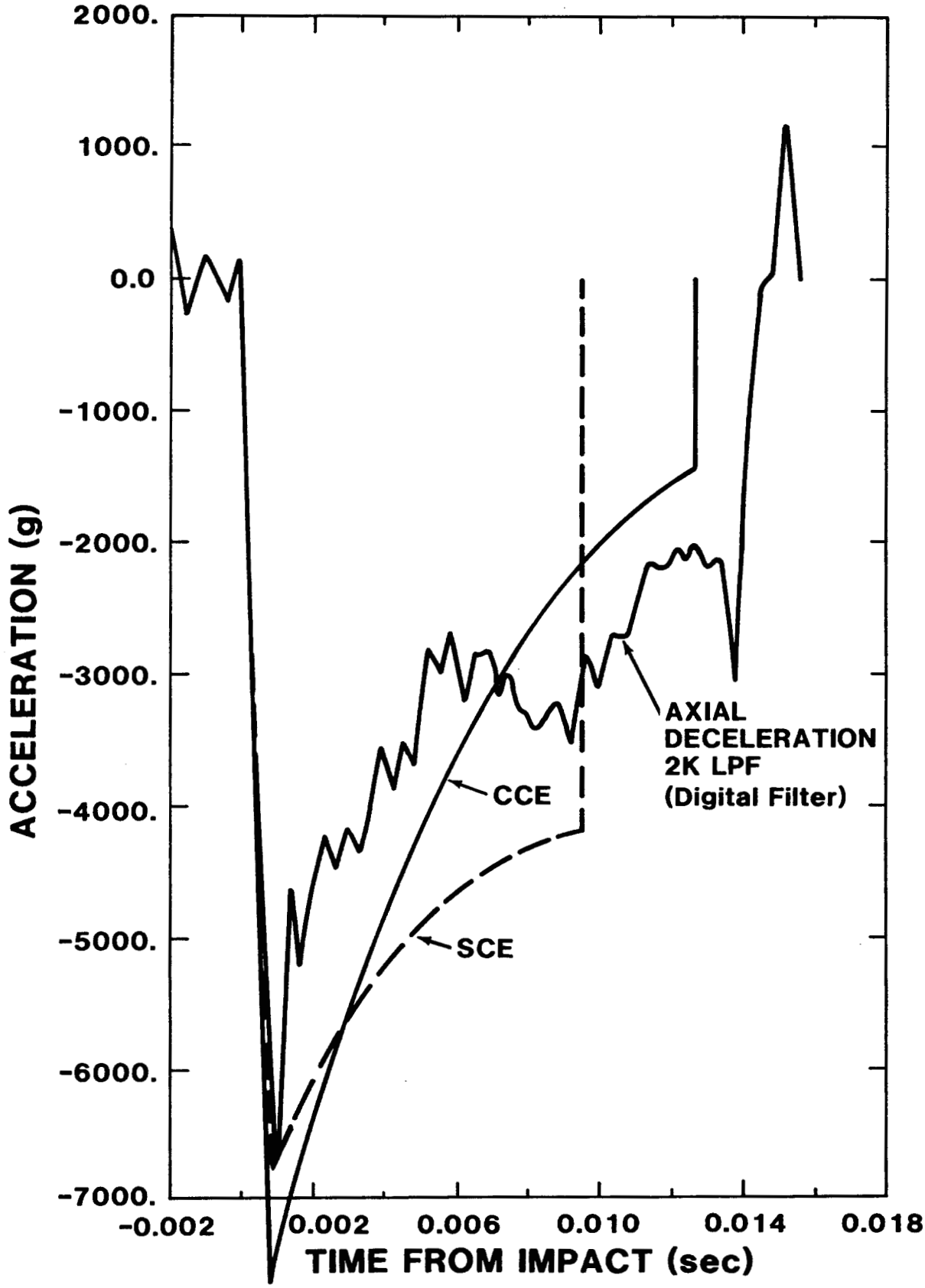

Figure 7. SCE and CCE Calculated and Measured Axial Deceleration for the SEPW-DG4 Test

APPENDIX - SOLUTION OF SPHERICAL CAVITY EXPANSION PROBLEMS

GOVERNING EQUATIONS

In analyzing the 1-D static and dynamic response of an infinite medium in which a spherical cavity is expanding from zero initial radius at constant radial velocity, both Lagrangian R and Eulerian r radial coordinates are employed. They are related by

$$r = R + u \tag{A1}$$

where u is the particle displacement in the radial direction. The difference in these coordinates is not usually important in the elastic region, Figure 4, but is obviously significant near the surface of the cavity which has expanded to finite radius r = a (at R = 0).

The target or medium response is generally separated into three regions - elastic, cracked, and plastic. These are separated by three radially propagating spherical interfaces at Eulerian coordinates $r = c_1 t$, $c_2 t$, and $c_3 t$ as shown in Figure 4.

The medium motion within each of these regions is governed by the equations of momentum and mass conservation in Lagrangian coordinates,

$$\rho_0 R^2 \frac{\partial^2 u}{\partial t^2} = - (R + u)^2 \frac{\partial \sigma_R}{\partial R} - 2(R + u) \left(1 + \frac{\partial u}{\partial R}\right) \left(\sigma_R - \sigma_\phi\right) \tag{A2}$$

$$\rho_0 R^2 = \rho (R + u)^2 \left(1 + \frac{\partial u}{\partial R}\right) \tag{A3}$$

where ρ_0, ρ are the initial and current densities and σ_R, σ_ϕ are the radial and tangential components of Cauchy stress, taken positive in compression.

The equations of conservation of momentum and mass across a moving spherical interface are required to connect the response in one region with

that in an adjacent area, e.g., across the elastic-cracked interface. These equations, for an interface moving in the positive r direction with speed c in an Eulerian frame are

$$\sigma_R^- - \rho^- v^- (c - v^-) = \sigma_R^+ - \rho^+ v^+ (c - v^+) \tag{A4}$$

$$\rho^- (c - v^-) = \rho^+ (c - v^+) \tag{A5}$$

where $v = \partial u/\partial t$ is the particle velocity and +, - refer to the radially outer and inner sides of the interface, respectively. Equations (A4, A5) are the same as those in cylindrical coordinates, Reference [2].

QUASISTATIC RESPONSE

When the spherical cavity growth is slow enough, corresponding to low penetration speeds, a quasistatic assumption is valid and leads to closed-form results for the stress required to expand the cavity. These results are useful in providing an independent check of the dynamic solution in the limit of zero cavity expansion velocity. The solution procedure is similar to that for cylindrical cavity expansion, Reference [2]. It will be summarized here for elastic-plastic response and the results given for both elastic-plastic and elastic-cracked-plastic response.

The medium response is assumed to consist of two regions, a plastic one, $a < r < r_1$ and an elastic one $r_1 < r$; where r_1 is the Eulerian coordinate of the elastic-plastic interface. Using results from Hill, Reference [10] for the elastic response of a medium with a spherical boundary surface and applying the Mohr-Coulomb condition of incipient plasticty, Equation [3] at $r = r_1^+$ gives the elastic results at the interface,

$$\sigma_{R_1}^{+} = \frac{2}{3}\tau_o \tag{A6}$$

$$\sigma_{\phi_1}^{+} = -\frac{\tau_o}{3} \tag{A7}$$

$$u_1^{+} = \frac{(1+\nu)\,\bar{\tau}_o\, r_1}{9(1-2\nu) + (1+\nu)\,\bar{\tau}_o} \qquad , \bar{\tau}_o = \tau_o/K \tag{A8}$$

Rewriting Equation (A2) in terms of r and omitting the inertia term gives the equation of static equilibrium. This is integrated to determine σ_R after using Equations (2, 3) to eliminate σ_ϕ. After satisfying continuity of σ_R at $r = r_1$, the stress at the cavity surface is

$$\sigma_R(a) = \tau_o \left[\left(\frac{2}{3} + \frac{1}{\mu} \right) \left(\frac{r_1}{a}\right)^{\left(\frac{2\mu}{1 + 2\mu/3} \right)} - \frac{1}{\mu} \right] \tag{A9}$$

The ratio r_1/a is determined by considering displacements. Equation (2) is used to substitute for ρ/ρ_o in the continuity Equation (A3) and following Chadwick [11] the result is written in terms of r and R using Equation (A1). This is integrated to give

$$\int_o^{r_1 - u_1} R^2 dR = \int_a^{r_1} \frac{r^2 dr}{1 - P/K} \tag{A10}$$

where P is known through Equations (A9,3). Using the small parameter $\bar{\tau}_o << 1$, an approximate solution to Equation (A10) is developed for r_1/a,

$$\left(\frac{a}{r_1}\right)^3 = \bar{\tau}_o \left\{ \frac{1-\nu}{1-2\nu} - \frac{\left(1 + \frac{2\mu}{3}\right)}{\mu} \left[\frac{(1-\nu)\bar{\tau}_o}{1-2\nu}\right]^{\frac{1}{1 + \frac{2\mu}{3}}} \right\} + \ldots \tag{A11}$$

As μ -> o, Equation (A9) can be evaluated by L'Hospital's rule, but Equation (A11) breaks down as the correction term becomes of the same order as the leading term and a different approximate expression is required.

Equations (A9, A11) give the stress required to expand a spherical cavity slowly from zero initial radius when the material is elastic-plastic. The most usual case for geologic materials is when Y << Q and an additional cracked region of response should be included. For this case, the results of an analysis similar to that given for the elastic-plastic case are

$$\sigma_R(a) = \frac{\tau_o}{\mu}\left[\left(\frac{1 + 2\frac{\mu}{3}}{1 - \frac{\mu}{3}}\right)\left(\frac{r_1}{a}\right)^{\left(\frac{2\mu}{1 + 2\frac{\mu}{3}}\right)} - 1\right] \tag{A12}$$

$$\left(\frac{a}{r_1}\right)^3 = 3\left(\frac{1 - \nu}{1 - 2\nu}\right)\left[2\left(1 - \frac{\mu}{3}\right)\right]^{-3/2}\left(\frac{\tau_o}{Y}\right)^{1/2}\bar{\tau}_o + \\ - \frac{\left(1 + \frac{2\mu}{3}\right)}{\mu\left(1 - \frac{\mu}{3}\right)}\bar{\tau}_o\left(\frac{a}{r_1}\right)^{\frac{3}{1 + 2\frac{\mu}{3}}} \tag{A13}$$

Equations (A12, A13) give the required stress to expand a spherical cavity when the medium response is elastic-cracked-plastic and approximate the stress on a penetrator nose at low velocity. As μ -> o, Equations (A12, A13) have the same limitations as discussed previously for Equations (A9, A11).

DYNAMIC ELASTIC-PLASTIC RESPONSE

For high enough cavity expansion velocity, tensile stresses in the target do not reach the tensile strength of the rock (σ_ϕ > - Y) and an elastic-plastic solution is valid. This is represented in Figure 4 if the cracked region between interfaces 1 and 2 is removed.

Elastic Response. Following Reference [9], Equation (A2) is linearized and written in terms of u using Hooke's law (with K, ν). The resulting equation is reduced to a first order equation in $dq/d\xi$ by the transformations

$$\xi = \frac{R}{c_1 t} \quad ; \; \bar{u} = \frac{u}{c_1 t} \quad ; \; q = \xi^{-1}\bar{u} \tag{A14}$$

where ξ is a similarity parameter and c_1 is the unknown speed of the elastic-plastic interface in an Eulerian frame. In the elastic region it is not necessary to distinguish between Lagrangian and Eulerian coordinates R and r. After satisfying $\bar{u} = 0$ at the elastic wave front ($\xi = 1/\gamma$, $\gamma = c_1/c_3$) and the Mohr-Coulomb condition (3) at the elastic-plastic interface $\xi = 1$ (the difference between Lagrangian and Eulerian coordinates may be neglected in the elastic region), the solution is

$$\bar{u} = B\left(\frac{-2\gamma^3\xi^3 + 3\gamma^2\xi^2 - 1}{3\gamma^2\xi^2}\right); \quad \frac{d\bar{u}}{d\xi} = \frac{2B\left(1 - \gamma^3\xi^3\right)}{3\gamma^2\xi^3} \tag{A15}$$

$$\bar{v} = \bar{u} - \xi\,\frac{d\bar{u}}{d\xi} \tag{A16}$$

$$\bar{\sigma}_R = -\frac{3}{(1+\nu)}\left[(1-\nu)\,\frac{d\bar{u}}{d\xi} + 2\nu\,\frac{\bar{u}}{\xi}\right] \tag{A17}$$

$$\bar{\sigma}_\phi = -\frac{3}{(1+\nu)}\left[\nu\,\frac{d\bar{u}}{d\xi} + \frac{\bar{u}}{\xi}\right] \tag{A18}$$

where

$$B = -\frac{(1+\nu)\,\gamma^2\,\bar{\tau}_0}{3(1-\gamma^2)\left[1 - 2\nu - \frac{2\mu(1+\nu)\gamma^2}{3(1+\gamma)}\right]} \tag{A19}$$

and $\bar{v} = v/c_1$; $\bar{\sigma}_R = \sigma_R/K$; and $\bar{\sigma}_\phi = \sigma/K$. In Equations (A15-19) γ is, at this point, unknown.

Elastic-Plastic Interface Conditions. Using the conditions (A4, A5) and applying the Mohr-Coulomb condition on both sides of the elastic-plastic interface, one finds that $\bar{u}$, $\bar{v}$ and all other quantities are continuous across this interface.

Plastic Response. Using Equations (2, 3, A3) to substitute into Equation (A2) and the transformation (A14) yields the field equation in the plastic region

$$\begin{aligned} &\left[\alpha^2\xi^6 - \left(1 + \frac{2}{3}\mu\right)\left(\xi + \bar{u}\right)^4\right]\frac{d^2\bar{u}}{d\xi^2} + \\ &+ 2\,(\xi + \bar{u})\left(1 + \frac{d\bar{u}}{d\xi}\right)\left\{\left(1 + \frac{2}{3}\mu\right)\left(\xi + \bar{u}\right)^2\left(\frac{\bar{u}}{\xi} - \frac{d\bar{u}}{d\xi}\right) + \right. \\ &\left. + \bar{\tau}_0\,\xi^2 - \mu\left[2\xi\bar{u} + \bar{u}^2 + (\xi + \bar{u})^2\frac{d\bar{u}}{d\xi}\right]\right\} = 0 \end{aligned} \tag{A20}$$

where $\alpha^2 = \alpha_1^2 = c_1^2/c_p^2$; $c_p^2 = K/\rho_0$. The nonlinear Equation (A20) is solved by an inverse numerical procedure beginning at the elastic-plastic interface $\xi = 1-\bar{u}_1^-$, and ending at the cavity surface $\xi = 0$ where 1 refers to the interface. New dependent variables

$$U = \bar{u} + \xi,\ N = \frac{1}{\xi^2}\ \frac{dU}{d\xi} \tag{A21}$$

are introduced to convert (A20) into a pair of first order equations which are solved by a Runge-Kutta integrating subroutine, Reference [12]. A value of the unknown constant α is assumed. With the restriction $\alpha^2 < 1 + 2\mu/3$ the coefficient of $d^2\bar{u}/d\xi^2$ will be negative and no singularity will occur. $\bar{u}_1^+$ and $\bar{v}_1^+$ from the elastic solution (A15-19) and continuity of $\bar{u}$ and $\bar{v}$ at $\xi = 1 - \bar{u}_1$ provide starting values for U and N. When the integration reaches $\xi = 0$ the cavity expansion velocity $\dot{a}$ corresponding to the assumed value of α is determined by

$$a = \dot{\alpha} c_p U(o) \tag{A22}$$

The corresponding normal stress required to expand the spherical cavity is

$$\sigma = K \left(1 + \frac{2}{3}\mu\right) \left[1 - U^2(0)\ N(0)\right] + \frac{2}{3}\ \tau_0 \tag{A23}$$

For identical input parameters representing sidewinder tuff ($\bar{\tau}_0$ = 0.00383, μ = 0.91, and υ = 0.21) we find that the limit of the dynamic solution as $\dot{a}$ --> 0 gives σ/K = 0.0458 while the quasistatic solution (9A,11A) gives σ/K = 0.0460, which is satisfactory agreement.

DYNAMIC ELASTIC-CRACKED-PLASTIC RESPONSE

At low enough cavity expansion velocity, the target is modeled with regions of elastic, cracked, and plastic response, as shown in Figure 4. In the cracked region, σ_ϕ = 0. This region is required because otherwise, σ_ϕ would exceed the material tensile strength.

Field Equations. Variables are non-dimensionalized based on the unknown speed of the cracked-elastic interface, c_2. In particular,

$$\xi = R/c_2 t \tag{A24}$$

In the elastic region, the solution is required to satisfy the condition

$$\sigma_\phi = -Y \tag{A25}$$

at the elastic side of the cracked-elastic interface, $R = c_2 t^+$. The elastic solution is again given by Equations (A14-A18) with c_1 replaced by c_2 and

$$B = \frac{(1 + \nu)\ \bar{Y}\ \gamma^2}{2\nu\ (1 - \gamma^3) + (-2\gamma^3 + 3\gamma^2 - 1)} \tag{A26}$$

where $\gamma = c_2/c_3$.

In the cracked region, the global effect of major tensile fractures is represented by

$$\sigma_\phi = 0 \tag{A27}$$

Using Equations (A27, 2, A3) and the transformation (A24) to substitute into Equation (A2) yields the field equation in the cracked region

$$\left[\alpha^2\xi^6 - 3(\bar{u} + \xi)^4 \right] \frac{d^2\bar{u}}{d\xi^2} - 6(\xi + \bar{u}) \left(1 + \frac{d\bar{u}}{d\xi} \right) \left[2(\xi + \bar{u})^2 \frac{d\bar{u}}{d\xi} + \right.$$

$$\left. + \xi\bar{u} - \bar{u}^2 - \frac{\bar{u}^3}{3} \right] = 0 \tag{A28}$$

The region of plastic response in which the Mohr-Coulomb condition (3) is satisfied is again represented by Equation (A20) in which $\alpha = \alpha_2 = c_2/cp$ and $\xi = R/c_2t$.

<u>Interface Conditions</u>. Initially, both the elastic-cracked and the cracked-plastic interface speeds are unknown. The solution at $\xi = \xi_2^+$ is known and in particular $\sigma_\phi = -Y$. Using these results and $\sigma_\phi = 0$ at $\xi = \xi_2^-$ in Equations (A4, A5, and 2) gives

$$\bar{v}_2^- = \frac{2\bar{Y}\,\bar{\rho}_2^+ \left(1 - \bar{v}_2^+\right) + 3\bar{v}_2^+ - \alpha_2^2 \left(\bar{\rho}_2^+\right)^2 \bar{v}_2^+ \left(1 - \bar{v}_2^+\right)^2}{3 - \alpha_2^2 \left(\bar{\rho}_2^+\right)^2 \left(1 - \bar{v}_2^+\right)^2} \tag{A29}$$

in which $\bar{v} = v/c_2$, $\bar{Y} = Y/K$, $\alpha_2 = c_2/c_p$, and $\bar{\rho} = \rho/\rho_0$. In equation (A29) $\bar{\rho}_2^+$ is computed from the known stresses and is not equal to 1. Equation (A29) represents a jump in $\bar{v}_2$ and other quantities have corresponding jumps.

At the cracked-plastic interface, ξ_1, a similar procedure shows all quantities are continuous. An additional condition used to determine the location of this interface in the solution procedure discussed below is

$$\bar{\sigma}_R = \frac{\bar{\tau}_0}{1 - \mu/3} \quad , \; \xi = \xi_1 \tag{A30}$$

which results from setting $\sigma_\phi = 0$ in Equation (3).

Solution Procedure. As for the elastic-plastic calculations, the field equations (A20, A28) are numerically integrated using the dependent variables U and N, Equation (A21). One difference is that now, both interface speeds c_1 and c_2 are unknown. The solution starts by assuming a value of c_2 (or $\alpha_2 = c_2/c_p$), and the numerical integration begins at the elastic-cracked interface, $\xi = \xi_2 = 1 - \bar{u}_2$. Using the known elastic solution, continuity of $\bar{u}$, and Equations (A29, A15, A16, A21), the starting values U_2^- and N_2^- are known. Then the numerical solution of U and N proceeds with ξ decreasing until Equation (A30) is satisfied which determines the cracked-plastic interface ξ_1. U and N are continuous at this interface and the numerical solution continues with U, N satisfying the plastic field equation (A20) until the cavity surface $\xi = 0$ is reached. To avoid singularities in the differential equations, α^2 is restricted by both $\alpha^2 = \alpha_2^2 < 1 + 2/3\mu$ and $\alpha^2 = \alpha_2^2 < 3$.

For input parameters representative of sidewinder tuff ($\bar{\tau}_0 = 0.00383$, $\mu = 0.91$, $\bar{Y} = 0.00036$, $\upsilon = 0.21$), the limit of the dynamic solution as $\dot{a}$ --> 0 gives $\sigma/K = 0.0322$ while the quasistatic solution (A12, A13) gives $\sigma/K = 0.0323$, which is satisfactory agreement.

USE OF THE SCE MODEL AS A LOAD SUBROUTINE IN GNOME

The SCE elastic-plastic and elastic-cracked-plastic numerical solution procedures have been implemented together as a load subroutine in the GNOME penetration code. Once a penetration problem is defined in GNOME, a curve of normal stress on the penetrator versus velocity normal to the penetrator surface is generated to cover the range of penetrator surface velocities. This curve is calculated once at the beginning of the penetration solution and then subsequently interpolated as needed to determine the load stresses on the penetrator during a complete trajectory calculation.

In determining the initial σ versus $\dot{a}$ curve, it is necessary to decide when to change from elastic-plastic target response (at high $\dot{a}$) to elastic-cracked-plastic response (at low $\dot{a}$). The criterion used is that elastic-plastic response occurs for values of $\alpha = \alpha_1 = c_1/c_p$ such that

$$\alpha_1 > \alpha^* \tag{A31}$$

$$\alpha^* = \frac{1}{2}\left[\frac{3(1-\nu)}{1+\nu}\right]^{1/2}\left[\delta + (\delta^2 + 4\delta)^{1/2}\right]$$

$$\delta = \frac{(1-2\nu)}{2(1+\nu)}\left[1 + \left(\frac{\mu - 3}{\tau_0 - \mu Y}\right)Y\right]$$

where c_1 is the elastic-plastic interface speed.

The criteria (A31) is developed from the equation $\sigma_\phi = -Y$, where σ_ϕ comes from the elastic solution (A18), evaluated at $\xi = 1$. The largest tensile stress always occurs at the elastic-plastic interface, $\xi = 1$.

To calculate σ at penetrator local normal velocity components lower than those for which $\alpha_1 > \alpha^*$, we assume elastic-cracked-plastic response and select values of $\alpha_2 = c_2/c_p$ such that $0 < \alpha_2 < \alpha^*$, where α_2 is the elastic-cracked interface speed. For elastic-cracked-plastic response, $\alpha_1 < \alpha_2$.

Distribution:

Francois Heuze, L-200
LLNL
Livermore, CA 94550

Prof. H. L. Schreyer
Mechanical Engineering Dept.
University of New Mexico
Albuquerque, NM 87131

1510	J. W. Nunziato
1520	L. W. Davison (2)
1521	H. S. Morgan
1522	R. C. Reuter, Jr.
1522	E. D. Reedy
1523	J. H. Biffle
1523	E. P. Chen
1524	D. R. Martinez
1524	D. B. Longcope (10)
1530	J. R. Asay
1550	C. W. Peterson
3141	S. A. Landenberger (5)
3154-1	C. L. Ward for DOE/OSTI (8)
3151	W. I. Klein (3)
5165	R. J. Kipp
7111	T. K. Bergstresser
7542	T. G. Priddy
7542	V. I. Bateman
9122	M. M. Hightower
9123	J. M. Holovka
9123	V. K. Luk
9123	C. W. Young
9123	E. R. Young
9145	A. K. Miller
8524	J. A. Wackerly